Experimental Characterization and Modeling of Low-Cost Oscillators for Improved Carrier Phase Synchronization

John McNeill, Sabah Razavi, Kirty Vedula, D. Richard Brown III
ECE Dept., Worcester Polytechnic Institute
Worcester, MA 01609-2280 e-mail: mcneill@wpi.edu

***Abstract*—Phase noise performance is measured for nine different crystal oscillators, each suitable for use as a frequency reference in applications such as software defined radio and coherent cooperative communication systems. The phase noise measurements are parametrically fit to a standard two-state oscillator model to characterize the short-term and long-term stability parameters of each oscillator. A three-state model is also developed to provide a better fit to the measured phase noise spectrum for some of the tested references. In addition to providing a better fit to the measured phase noise spectra, the three-state model enables improved phase estimation and prediction performance. A numerical example is presented in which a Kalman filter derived from the three-state model shows up to 3 dB improvement in mean squared error compared with the two-state model.**

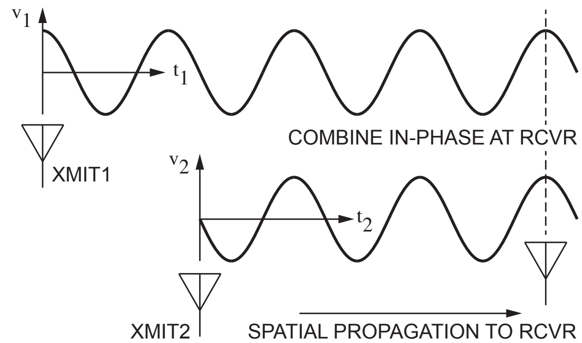

Fig. 1. Conceptual beamforming.

I. Introduction

Characterization and modeling of clock oscillator stability is important for many applications requiring an accurate time and/or frequency reference. This paper focuses on the application area of cooperative communication protocols [1]–[4], in which two or more sources transmit simultaneously in a single subchannel. A key challenge is maintaining synchronization between transmitters to picosecond accuracy, which in turn requires characterizing the stability of the independent frequency references for each transmitter.

Oscillator stability has been traditionally characterized by the Allan variance and multistate stochastic models [5]–[7] which were originally developed for high precision, high cost sources such as atomic clocks. Knowledge of model parameters allows development of tracking and prediction techniques (e.g. based on the Kalman filter) which enable accurate prediction of and compensation for oscillator drift.

Difficulty arises in applying these techniques to low cost, moderate precision crystal oscillators used in applications such as software-defined radio (SDR), as significant deviations in measured phase noise from the prediction of models in [6], [7] are observed for some oscillators. For the novel contributions of this paper, we present measured phase noise data for a range of crystal oscillators, propose an alternative phase noise modeling strategy, and show improved phase tracking and prediction performance resulting from the proposed model.

This paper is organized as follows: Section II provides background on cooperative communication and oscillator stability considerations for the SDR platform. Section III reviews previous work on a two-state model for oscillator noise, and the relationship between characterization through measurement and the resulting model parameters. In Section IV, a survey of measured phase noise for a range of crystal oscillators shows that some sources exhibit a characteristic that cannot be represented adequately by the two-state model, motivating development of a three-state noise model. Results when the three-state model is applied to phase error tracking and prediction are presented in Section V.

II. Background

A. Cooperative communication

In cooperative communication protocols, two or more sources transmit simultaneously in the same subchannel [1]–[4]. Figure 1 shows a conceptual view of the beamforming principle, in which the individual transmitter carrier waveform phases are adjusted to arrive in-phase at the receive antenna. Compared to to orthogonal transmit cooperation, these protocols offer the potential for improved power efficiency since carrier signals from each source arrive in phase and constructively combine at the intended destination. The key challenge to realizing these benefits is maintaining strict synchronization between transmitters: Phase offset must be less than a fraction of the carrier waveform, of order picoseconds for commonly used SDR frequencies.

Figure 2 from [2] shows the need for continuously updated phase realignment. This figure shows beamforming gain in a

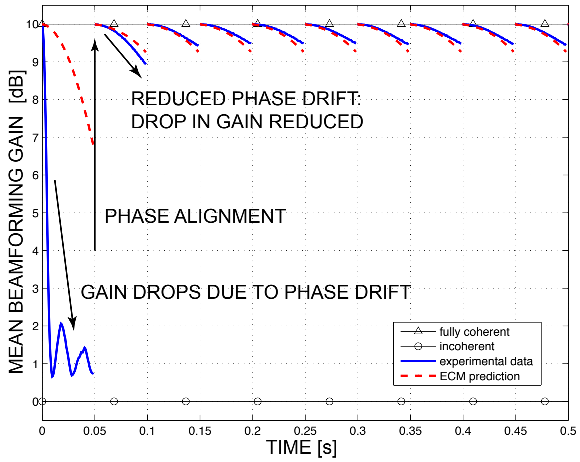

Fig. 2. Need for clock resynchronization.

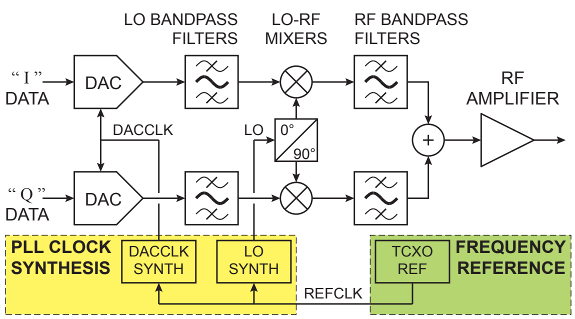

Fig. 3. SDR simplified block diagram.

three-source system over time, with a gain of 0 dB corresponding to incoherent transmission and a theoretical maximum gain of 10 dB. At time $t = 0$ the oscillators are synchronized and gain of 10 dB is briefly observed, but gain quickly drops near zero in less than 10 ms as the source oscillator phases drift out of phase alignment. Interrupting channel usage for phase measurement and realignment on a millisecond time scale would detract significantly from the achievable system data rate, adding an unacceptable overhead in data transmission.

To extend the amount of time available between necessary phase realignments, phase error prediction is also used. At $t = 50$ ms the oscillator phases are realigned, and based on the observed oscillator behavior, the phase error drift of each source oscillator is predicted and partially canceled. Due to unpredictable random drift, the observed beamforming gain decreases over time, in this case to approximately 9 dB by the next resynchronization at $t = 100$ ms. With prediction, the allowable time between phase realignment is extended to 50 ms in this example.

The following section describes sources of phase noise and oscillator drift for SDRs used in cooperative communication.

B. SDR output phase noise

Figure 3 shows a simplified block diagram of a software-defined radio as implemented in the USRP-2 [8] platform. Precise frequency reference is required for both the baseband digital-to-analog converter (DAC) functions (400 MS/s clock DACCLK) and the local oscillator (LO) synthesizer which upconverts the I/Q baseband data signals for transmitting at RF. In [8] the frequency reference is provided by a temperature compensated crystal oscillator (TCXO), which will influence the spectral characteristics of the RF output.

Figure 4 shows the measured phase noise of the USRP output when producing a continuous unmodulated 900 MHz carrier. (All measurements in this work were performed using the Keysight E5052B Signal Source Analyzer [9]). As described in [10], [11], the output phase noise is a combination of contributions from the reference oscillator (green highlight) and the phase-locked loop (PLL) synthesizer (yellow). At offset frequencies above $\approx$ 10 kHz, noise power is dominated by the PLL synthesizer's voltage-controlled oscillator (VCO) phase noise as well as spurs due to DAC quantization noise and nonlinearity. For synchronization purposes, we are concerned with oscillator drift at time scales of $\approx 100\,\mu$s and longer, which is determined by noise power at offset frequencies below 10 kHz. At offset frequencies $<$ 10 kHz performance is dominated by the REF source, and shows two regions with

- -40 dB/decade slope corresponding to a $1/f^4$ noise power law for offset frequencies $f < 100$ Hz, and
- -20 dB/decade slope corresponding to a $1/f^2$ noise power law for offset frequencies $100\text{ Hz} < f < 10\text{ kHz}$.

The $1/f^4$ and $1/f^2$ noise power laws follow from a simple model for oscillator phase noise, which will be briefly reviewed in the following section.

III. Oscillator Noise Modeling

A. Two-state oscillator phase noise model

In [6], the output of a sinusoidal oscillator is modeled as

$$u(t) = U_0 \sin\left(2\pi\nu_0 t + \varphi(t)\right) \tag{1}$$

in which ν_0 is the nominal frequency, $\varphi(t)$ is an error term due to oscillator phase noise, and U_0 is the oscillator amplitude. Any effects due to variation in U_0 are assumed to be negligible since the analysis considers phase noise only; for this reason

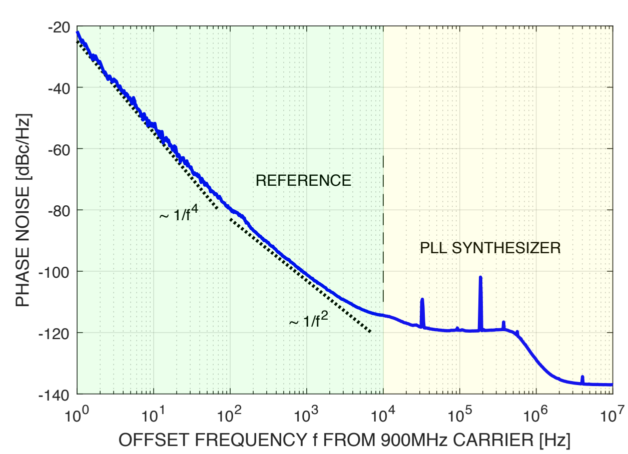

Fig. 4. Measured phase noise of USRP carrier output.

the analysis also applies to nonsinusoidal oscillators such as the frequency reference used in [8].

In (1) the error $\varphi(t)$ has units of radians of phase. This error can be expressed in terms of time error $x(t)$ by normalizing to the nominal radian frequency

$$x(t) = \frac{\varphi(t)}{2\pi\nu_0} \tag{2}$$

with which (1) becomes

$$u(t) = U_0 \sin 2\pi\nu_0 \left(t + x(t)\right) \tag{3}$$

In [6] it is shown that the output noise process can be modeled by a simplified two-state system shown in graphical form in Figure 5 and expressed mathematically as

$$x(t) = x_1(t) = \int_0^t \left(x_2(t) + \xi_1(t)\right) dt \tag{4}$$

$$x_2(t) = \int_0^t \xi_2(t) dt \tag{5}$$

in which $\xi_1(t)$ and $\xi_2(t)$ are noise processes. As a time error, x_1 has units of seconds [s]; due to the time derivative to $\dot{x}_1$, x_2 and ξ_1 are dimensionless. Similarly, the units of ξ_2 are [s^{-1}].

Expressing the system of Fig. 5 in state space form gives:

$$\underbrace{\begin{bmatrix} \dot{x}_1 \\ \dot{x}_2 \end{bmatrix}}_{\dot{\mathbf{x}}} = \underbrace{\begin{bmatrix} 0 & 1 \\ 0 & 0 \end{bmatrix}}_{\mathbf{A}} \underbrace{\begin{bmatrix} x_1 \\ x_2 \end{bmatrix}}_{\mathbf{x(t)}} + \underbrace{\begin{bmatrix} \xi_1 \\ \xi_2 \end{bmatrix}}_{\xi\mathbf{(t)}} \tag{6}$$

As in [6], we model the process noise terms $\xi_1(t)$ and $\xi_2(t)$ as zero mean independent Gaussian random processes. Since the process are independent, the autocorrelation is

$$\mathbf{R}_{\xi,\xi}(\tau) = E\left[\xi(t)\xi^T(t+\tau)\right] = \underbrace{\begin{bmatrix} q_1 & 0 \\ 0 & q_2 \end{bmatrix}}_{\mathbf{Q}} \delta(\tau) \tag{7}$$

where $\delta(\tau)$ is the Dirac delta function.

From (4) and (5) with the noise model of (6),we expect the power spectral density to exhibit a $1/f^2$ region corresponding to a Wiener process from the integration of $\xi_1(t)$, and a $1/f^4$ region corresponding to the integration of $x_2(t)$, which is itself a Wiener process as the integral of $\xi_2(t)$. Table I lists all reference sources evaluated for this paper. As an example, measured data from CS4 at a frequency of $\nu_0 = 40\,\text{MHz}$ in Fig. 6 shows a phase noise plot $\mathcal{L}(f)$ with approximate $1/f^4$ and $1/f^2$ characteristics until reaching the noise floor of the measurement.

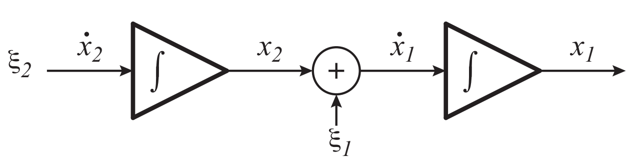

Fig. 5. 2-state clock noise model

In accordance with [5] we can model the single-sided spectral density of phase fluctuations as

$$S_\phi(f) = 2\mathcal{L}(f) = \frac{h_{-2}\nu_0^2}{f^4} + \frac{h_0\nu_0^2}{f^2} \tag{8}$$

with best-fit values to the measured $\mathcal{L}(f)$ for parameters h_{-2} and h_0 as shown in Fig. 6. Note that there are also $1/f$ and $1/f^3$ regions corresponding to flicker ($1/f$) and integrated flicker ($1/f^3$) noise respectively. For simplicity these models were not incorporated in this work, but could be taken into account for a more accurate description of phase noise.

To fully describe the system of Fig. 5, we need numerical values for q_1 and q_2 which describe the random processes. In [6], [7] these are obtained from the Allan variance $\sigma_y^2(\tau)$, a commonly used measurement for extremely stable clock sources [5]. For the two-state model of Fig. 5, [6], [7] shows that the Allan variance will take the form

$$\sigma_y^2(\tau) = \frac{q_1}{\tau} + \frac{q_2\tau}{3} \tag{9}$$

The Allan variance (time domain) can be related to the phase noise (frequency domain) using expressions in [5]. For the two state noise model, [5] gives a form of

$$\sigma_y^2(\tau) = \frac{h_0}{2\tau} + \frac{2\pi^2 h_{-2}\tau}{3} \tag{10}$$

Equating coefficients in (9) and (10) gives

$$q_1 = \frac{h_0}{2} \quad q_2 = 2\pi^2 h_{-2} \tag{11}$$

Figure 6 shows the best-fit parameters for the two-state model given the measured noise performance.

B. Role of oscillator model in phase prediction

One value of the oscillator noise model is its role in determining a filter for prediction of oscillator phase error over time. Although the noise sources ξ_1 and ξ_2 are uncorrelated white noise sources, the integration in the model of Fig. 5 imposes a correlation in the output error $x(t)$ that can be utilized in predicting future evolution of oscillator error.

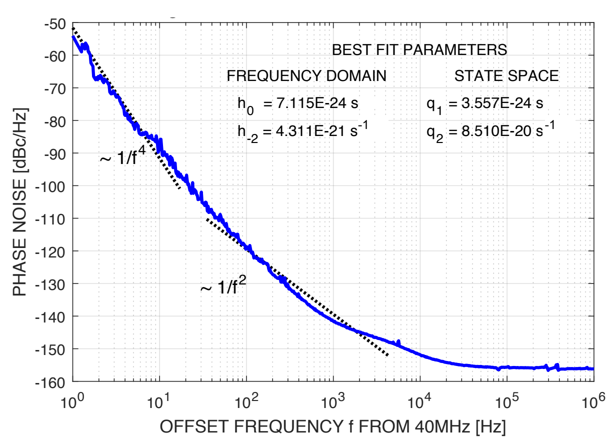

Fig. 6. Measured phase noise for oscillator CS4 with 2-state model fit.

TABLE I
CLOCK SOURCES EVALUATED IN THIS WORK

Source	Type	Brand	ν_0 [MHz]
CS1	VCXO	A	40
CS2	VCXO	A	100
CS3	XO	B	80
CS4	XO	B	40
CS5	OCXO	C	40
CS6	TCXO	C	40
CS7	XO	D	40
CS8	TCXO	E	100
CS9	VCXO	F	40

Key to Oscillator Type	
XO	Crystal Oscillator
TCXO	Temperature Compensated XO
OCXO	Oven Controlled XO
VCXO	Voltage Controlled XO

In [2] it is shown that optimal minimum mean squared error (MSE) phase tracking and prediction can be achieved with a Kalman filter derived from the state-space model of the phase noise process. Since the Kalman filter operates in discrete time on measured samples of oscillator phase error, the continuous time model of (6) is converted to a discrete time model subject to the time interval between relative phase error measurements.

It is important to note that the size of the Kalman gain matrix is set by the number of states in the oscillator noise model. The results in Fig. 2 were obtained using a 2 × 2 Kalman gain matrix resulting from the two-state noise model described in section III-A.

IV. THREE-STATE OSCILLATOR MODEL

A. Survey of crystal oscillators

To investigate the applicability of the two-state model, phase noise performance was measured for a range of low-cost crystal oscillators suitable for use as the frequency reference in an SDR application. The oscillators tested are given in Table I and measured characteristics are shown in Fig. 8. For offset frequencies below $\approx$ 100 Hz, all of the plots show behavior consistent with the two-state model. At higher offset frequencies, however, oscillators CS7 and CS8 show additional noise power beyond what could be predicted by a two-state model. Since tracking and prediction behavior in the cooperative communication application can rely on offset frequencies up to $\approx$ 10 kHz, it is important to modify the two-state model to model the extra noise power and allow development of an appropriate Kalman filter.

B. Development of three-state model

The shape of excess noise power in the phase noise plots for oscillators CS7 and CS8 is similar to the phase noise of the synthesized SDR output shown in Fig. 4. Indeed, the approach we will take in modeling the system for oscillators CS7 and CS8 is to assume that a phase-locked loop synthesizer is used to develop the output clock frequency. Figure 7 shows the proposed three-state model, with the previous two-state clock model as the input to a PLL synthesizer [10].

Since the controlled variable in a PLL is phase, the output state x_1 must be multiplied by $2\pi\nu_0$ to convert the time variable x_1 in seconds to an equivalent phase in radians at the PLL input. The voltage controlled oscillator (VCO) is represented with an integrator, since phase is the integral of frequency. Two parameters characterize the VCO for purposes of state space modeling:

- For consistency with the noise representation in the 2-state oscillator model, VCO phase noise is modeled as a white noise input $\xi_3(t)$ with units rad/s.
- The loop bandwidth of the PLL response is determined by time constant τ_L.

The block diagram for clock multiplication PLL synthesis as described in [10] usually shows a divide-by-N in the PLL feedback path, to accomplish the frequency multiplication by N from input to output. In this case the effect of $1/N$ in the feedback is reflected in scaling of τ_L and other signal sources in the block diagram.

Expressing the system of Fig. 7 in state space form gives:

$$\underbrace{\begin{bmatrix}\dot{x}_1\\ \dot{x}_2\\ \dot{x}_3\end{bmatrix}}_{\dot{\mathbf{x}}} = \underbrace{\begin{bmatrix}0 & 1 & 0\\ 0 & 0 & 0\\ \frac{2\pi\nu_0}{\tau_L} & 0 & \frac{-1}{\tau_L}\end{bmatrix}}_{\mathbf{A}} \underbrace{\begin{bmatrix}x_1\\ x_2\\ x_3\end{bmatrix}}_{\mathbf{x}} + \underbrace{\begin{bmatrix}\xi_1\\ \xi_2\\ \xi_3\end{bmatrix}}_{\xi(\mathbf{t})} \tag{12}$$

with output x_3 now in units of radians of phase.

C. Determining PLL parameters

As in [6], we model the new process noise term $\xi_3(t)$ as a zero mean independent Gaussian random process; now the $\mathbf{Q}$ matrix in the autocorrelation of (7) is

$$\mathbf{Q} = \begin{bmatrix}q_1 & 0 & 0\\ 0 & q_2 & 0\\ 0 & 0 & q_3\end{bmatrix} \tag{13}$$

The new model parameters q_3 and τ_L can be determined from the phase noise plot. From Fig. 7 the transfer function

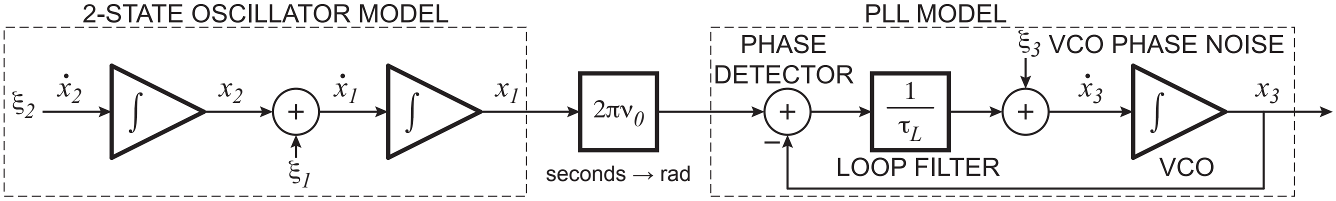

Fig. 7. Three-state model for phase noise of source with PLL synthesizer

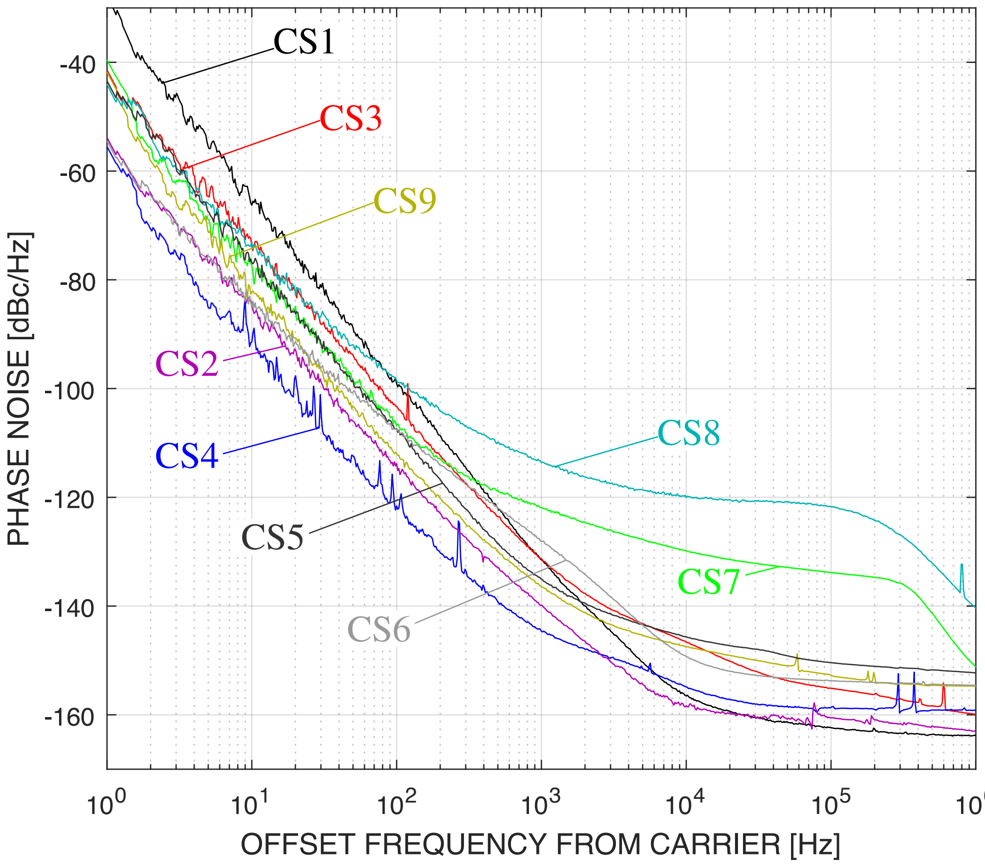

Fig. 8. Summary of phase noise measurements.

from ξ_3 to x_3 is

$$x_3 = \left(\frac{\tau_L}{1 + s\tau_L} \right) \xi_3 \tag{14}$$

Since ξ_3 is a white noise source, we expect from (14) to see a lowpass characteristic in the output phase noise due to ξ_3, which is observed in the measured phase noise of Fig. 9.

To account for the lowpass phase noise power spectral density, we add a lowpass term to (8)

$$S_\phi(f) = 2\mathcal{L}(f) = \frac{h_{-2}\nu_0^2}{f^4} + \frac{h_0\nu_0^2}{f^2} + \frac{h_v}{1 + (f/f_L)^2} \tag{15}$$

For q_3 describing the variance of ξ_3, using the square of the magnitude of the transfer function in (14) and equating coefficients with (15) gives

$$\tau_L = \frac{1}{2\pi f_L} \quad q_3 = \frac{h_v}{\tau_L^2} \tag{16}$$

Figure 9 shows the best-fit parameters for the three-state model given the measured noise performance for oscillator CS8.

V. Results

To test the applicability of the three-state model, a Kalman filter was defined using (12) with parameters from Fig. 9 for oscillator CS8. A Monte Carlo approach was used to generate simulated phase error waveforms with noise power as shown

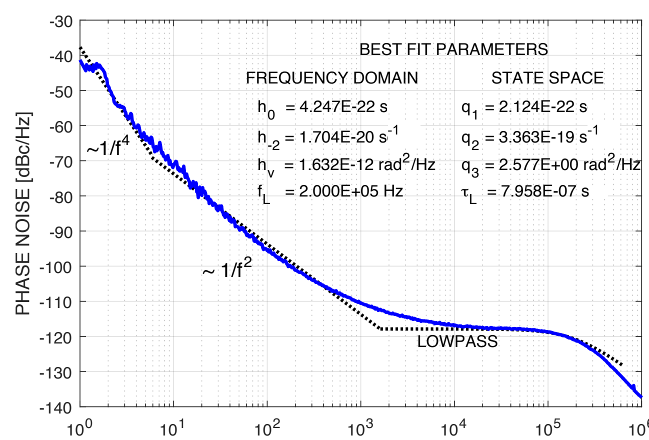

Fig. 9. Measured phase noise for oscillator CS8 with 3-state model fit.

in Fig. 9. Phase error was sampled at a 2 MHz rate to capture dynamics up to the 1 MHz offset frequency in Fig. 9.

Figure 10 shows sample waveforms for a prediction time of 10 μs. The three-state filter prediction (red) was compared to a two-state filter (blue) using only the q_1 and q_2 parameters corresponding to the low-offset-frequency region in Fig. 9. To emphasize oscillator modeling, no measurement noise was included. Figure 10(a) shows the behavior of both filters

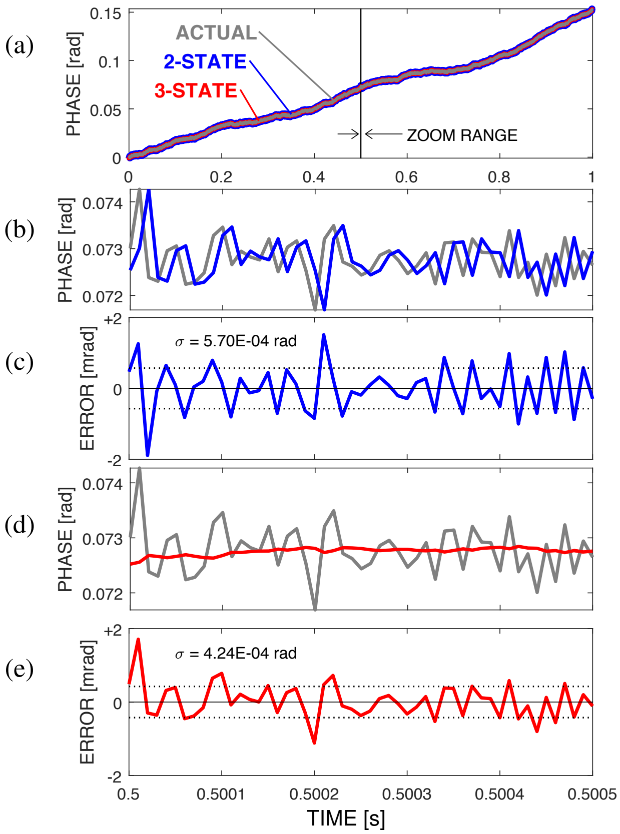

Fig. 10. Prediction for oscillator CS8 with 2- and 3-state model fits.

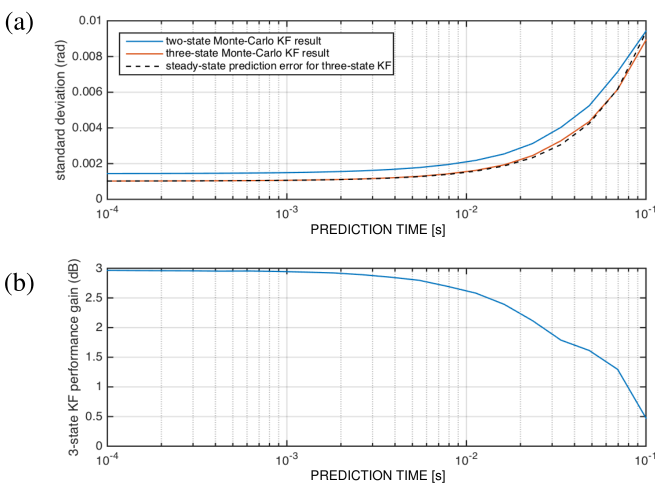

Fig. 11. Relative performance, 2-state vs. 3-state model fit.

relative to the actual phase error over a time scale of seconds. Both filters track the long term phase error closely, as expected since both filters share the two states corresponding to the low offset frequency ($1/f^4$ and $1/f^2$) phase noise asymptotes in Fig. 9.

Figure 10(b) shows the prediction (blue) and actual phase (gray) for the two-state filter; prediction error is shown in Fig. 10(c). Figs. 10 (d) and (e) show the prediction and error for the three-state filter; in the case of this particular waveform the MSE is improved by 2.9 dB over the two-state filter.

Figure 11(a) shows the standard deviation (averaged over the Monte Carlo ensemble) for both filters over a range of prediction times from 100 μs to 100 ms. As expected, error increases with prediction time, but at all times the three-state filter error is smaller. Figure 11(b) shows that the three-state filter advantage exceeds 2.5 dB for prediction times up to 10 ms; for longer prediction times the advantage is less pronounced as the performance of both predictors is degraded.

VI. Conclusion

A survey of widely available, low-cost oscillators shows two distinct types of shape for the frequency domain characteristic of phase noise performance. For oscillators exhibiting a phase noise density similar to that of a PLL synthesizer architecture, the traditional two-state model yields suboptimal performance in phase tracking and prediction. The proposed three-state model is shown to provide up to 3 dB improvement in MSE of prediction.

Acknowledgment

This material is based upon work supported by the National Science Foundation under grants ECS-0523996, ECCS-1232085, CCF-1302104, and CCF-1319458; and by the U.S. Army Defense University Research Instrumentation Program grant W911NF-16-1-0176. The authors also thank Keysight Technologies, Analog Devices, and Allegro Microsystems.

References

[1] D. R. Brown, G. B. Prince, and J. A. McNeill, “A method for carrier frequency and phase synchronization of two autonomous cooperative transmitters,” *2005 IEEE Workshop on Signal Processing Advances in Wireless Communications*, p. 260, Jun 2005.

[2] R. David, “Improving Channel Estimation and Tracking Performance in Distributed MIMO Communication Systems.” Ph.D. Dissertation, Worcester Polytechnic Institute, 2015.

[3] P. Bidigare et al., “Implementation and demonstration of receiver-coordinated distributed transmit beamforming across an ad-hoc radio network.” *ASILOMAR2012*, pp. 222-226

[4] F. Quitin et al., “Demonstrating distributed transmit beamforming with software-defined radios.” *2012 IEEE International Symposium on World of Wireless, Mobile and Multimedia Networks (WoWMoM)*, 2012.

[5] IEEE Standard 1139-2008, “IEEE Standard Definitions of Physical Quantities for Fundamental Frequency and Time Metrology,” 2008.

[6] L. Galleani, “A tutorial on the two-state model of the atomic clock noise.” *Metrologia*, vol. 45, no. 6, 2008.

[7] C. Zucca and P. Tavella, “The clock model and its relationship with the Allan and related variances,” *IEEE Trans. UFFC,* vol. 52, no. 2 (2005), pp.289-296.

[8] “USRP products,” E312 http://www.ettus.com, accessed 2016.

[9] Keysight E5052B Signal Source Analyzer

[10] J. A. McNeill and D. Ricketts, “The Designer’s Guide to Jitter in Ring Oscillators.” Springer, 2009.

[11] J. McNeill, “A Simple Method for Relating Time- and Frequency-Domain Measures of Oscillator Performance,” *Proc. 2001 IEEE Southwest Symp. Mixed Signal Design (SSMSD2001)*, Austin, TX, Feb., 2001.